Journal of Proteomics 196 (2019) 69–80

Contents lists available at ScienceDirect

Journal of Proteomics

journal homepage: www.elsevier.com/locate/jprot

Chronic exposure of bumblebees to neonicotinoid imidacloprid suppresses the entire mevalonate pathway and fatty acid synthesis

Tomas Erban[a,*], Bruno Sopko[a,b], Pavel Talacko[c], Karel Harant[c], Klara Kadlikova[a,d], Tatana Halesova[e], Katerina Riddellova[e], Apostolos Pekas[f]

[a] Crop Research Institute, Drnovska 507/73, Prague CZ-161 06, Czechia
[b] Department of Medical Chemistry and Clinical Biochemistry, Faculty of Medicine, Charles University and Motol University Hospital, V Uvalu 84/1, Prague CZ-150 06, Czechia
[c] Proteomics Core Facility, Faculty of Science, Charles University, Prague, Czechia
[d] Department of Plant Protection, Faculty of Agrobiology, Food and Natural Resources, Czech University of Life Sciences Prague, Kamycka 129, Prague 6, Suchdol CZ-165 00, Czechia
[e] ALS Limited, ALS Czech Republic, Na Harfe 336/9, Prague CZ-190 00, Czechia
[f] R&D Department, Biobest Group, Ilse Velden 18, Westerlo B-2260, Belgium

ARTICLE INFO

Keywords:
Imidacloprid-olefin
Pesticide exposure
Endocrine disruptor
Bombus terrestris
Proteomics
Terpenoid backbone biosynthesis pathway

ABSTRACT

Determining the side effects of pesticides on pollinators is an important topic due to the increasing loss of pollinators. We aimed to determine the effects of chronic sublethal exposure of the neonicotinoid pesticide imidacloprid on the bumblebee *Bombus terrestris* under laboratory conditions. The analytical standard of imidacloprid in sugar solution was used for the treatment. Verification of pesticides using UHPLC-QqQ-MS/MS in the experimental bumblebees showed the presence of only two compounds, imidacloprid and imidacloprid-olefin, which were found in quantities of 0.57 ± 0.22 and 1.95 ± 0.43 ng/g, respectively. Thus, the level of the dangerous metabolite imidacloprid-olefin was 3.4-fold higher than that of imidacloprid. Label-free nanoLC-MS/MS quantitative proteomics of bumblebee heads enabled quantitative comparison of 2883 proteins, and 206 proteins were significantly influenced by the imidacloprid treatment. The next analysis revealed that the highly downregulated markers are members of the terpenoid backbone biosynthesis pathway (KEGG: bter00900) and that imidacloprid treatment suppressed the entire mevalonate pathway, fatty acid synthesis and associated markers. The proteomics results indicate that the consequences of imidacloprid treatment are complex, and the marker changes are associated with metabolic and neurological diseases and olfaction disruption. This study provides important markers and can help to explain the widely held assumptions from biological observations. *Significance:* The major finding is that all markers of the mevalonate pathway were substantially downregulated due to the chronic imidacloprid exposure. The disbalance of mevalonate pathway has many important consequences. We suggest the mechanism associated with the novel toxicogenic effect of imidacloprid. The results are helpful to explain that imidacloprid impairs the cognitive functions and possesses the delayed and time cumulative effect.

1. Introduction

In the last decade, a pesticide class called neonicotinoids has become a common target of scientific investigation because these pesticides, which are highly toxic to insects, constitute a serious danger to pollinators through nectar and pollen transfer [1–6]. Due to concern that highly toxic neonicotinoids contribute to honeybee losses, the European Commission (EC) severely restricted imidacloprid, thiamethoxam and clothianidin under Regulation No 485/2013 of 24 May 2013 beginning December 1, 2013 [7]. The decision was made according to the outcomes of a scientific report by the European Food Safety Authority (EFSA) [8], and the moratorium in the European Union (EU) continues due to the subsequent evaluation that ended in February 2018; see the regulations 2018/783-785 of 29 May 2018 [9]. However, these systemic pesticides are still used in many other countries outside the EU, and risk assessment studies are still essential for policy decisions in both non-EU and EU countries. Moreover, the molecular mechanisms of the side effects are not understood.

* Corresponding author at: Proteomics and Metabolomics Laboratory, Crop Research Institute, Drnovska 507/73, Prague, CZ-16106, Czechia.
E-mail address: arachnid@centrum.cz (T. Erban).

https://doi.org/10.1016/j.jprot.2018.12.022
Received 27 September 2018; Received in revised form 7 December 2018; Accepted 20 December 2018
Available online 21 December 2018
1874-3919/

Imidacloprid is the most efficient neonicotinoid with excellent toxicity against various insect pests; however, there is a disadvantage in that its toxicity to bees is also high. Imidacloprid together with its metabolites can persist in the environment in significant amounts for years [10]. Thus, due to translocation from soil to plant tissues, pollen and nectar [1–4,6,11], the danger for pollinators can continue even in countries in which a ban has been applied. Field realistic pollen and nectar contamination can be on the order of a few μg per kg [1–3,5,6]. In honeybees, the acute LD_{50} of imidacloprid varies between 5 and 500 ng/bee, probably as a result of detoxification capacity [12], and the acute oral LD_{50} in bumblebees was determined to be 40 and 20 ng per bumblebee after 24 and 72 h of exposure, respectively [13]. Recent studies have indicated that imidacloprid causes different adverse effects on pollinators, with delayed and time-cumulative toxicity of imidacloprid observed in honeybees [14,15]. According to Dively et al. [15], honeybee colonies exposed to 20 and 100 μg imidacloprid per kg pollen experienced higher rates of queen failure and broodless periods. Bortolotti et al. [16] showed that sublethal imidacloprid doses influence the homing rate and foraging activity of honeybees. Decourtye et al. [17,18] showed that imidacloprid impairs honeybee olfactory learning and memory. Furthermore, Williamson and Wright [19] indicated that sublethal dose of imidacloprid impacted long-term memory. More recently, Ciereszko et al. [20] reported negative influences of imidacloprid on honeybee drone sperm quality. A negative effect of imidacloprid exposure on size of hypopharyngeal glands and extended cell death expression were observed by Smodis Skerl and Gregorc [21]. In *Bombus terrestris*, laboratory feeding of workers with a dose of 10 μg of imidacloprid per 1 kg of syrup and 6 μg of imidacloprid per 1 kg of pollen reduced brood production and lowered larval ejection [22]. More recently, Whitehorn et al. [23] observed reduced colony growth and an 85% reduction in production of *B. terrestris* queens after imidacloprid exposure of 6 μg/kg and 0.7 μg/kg or double these doses in pollen and sugar water, respectively. Also, other studies have indicated that field realistic imidacloprid doses decrease colony strength and condition [24,25]. The most recent biological observation using cameras by Crall et al. [26] showed that bumblebees exposed to imidacloprid at a dose of 1 ng per bee exhibited disrupted behavior and were less active in the nest. Effects on thermoregulation were also observed. An adverse impact of imidacloprid on behavior was observed by Parkinson et al. [27] in another insect, *Locusta migratoria*, in which visual processing and collision avoidance behavior were impaired by a sublethal dose 10 ng of imidacloprid per g of body weight.

Despite the high number and variety of studies based on biological observations, the molecular-level consequences of sublethal chronic doses of imidacloprid on bumblebees have not been elucidated. Some studies have sought to show the mechanism of neonicotinoid impact on bees. According to Manjon et al. [28], honeybees and bumblebees respond to various neonicotinoids differently, and the CYP9Q subfamily of cytochrome P450 determines the sensitivity of bees to neonicotinoids. In a study by Brandt et al. [29], thiacloprid and clothianidin exposure led to immunosuppression in honeybee queens. Other studies have indicated deregulation of proteins and/or transcripts. Dondero et al. [30] observed sublethal effects of imidacloprid and thiacloprid and their mixture on transcripts and proteins in the marine mussel *Mytilus galloprovincialis*. Meng et al. [31] performed 2D-*E*-MS/MS and identified 25 differentially expressed proteins between imidacloprid-resistant and -susceptible *Myzus persicae*, and in another study, Rix et al. [32] showed that sublethal imidacloprid doses can induce reproduction hormesis and alter the expression of detoxification genes in *M. persicae*. Furthermore, Pan et al. [33] compared thiamethoxam-resistant and -susceptible strains of *Aphis gossypii* in a transcriptomic study.

This study provides evidence at the proteome level that imidacloprid exposure suppresses a series of key enzymes in the terpenoid backbone metabolic pathway and fatty acid synthesis in bumblebee heads. Furthermore, we verify experimentally that bumblebees maintain the dangerous metabolite imidacloprid-olefin. Finally, we predict the cause of proteome changes in an *in silico* experiment. Overall, we provide for the first time indices for elucidating the mechanism of the adverse effects of imidacloprid on bumblebees.

2. Materials and methods

2.1. Biological samples and experimental design

The bumblebee *B. terrestris* nest Mini Hives and pollen were obtained from Biobest (Westerlo, Belgium). The care-free nutrition system in the Mini Hive was closed, and the hive was placed in a box equipped with an automatic parrot bird feeder, which provided a sugar diet and imidacloprid exposure. Moreover, there was round, netted opening in the upper lid of the box, which was used to supply pollen using a tweezer. Additional fabric was placed in the box to provide building material for the colony. After one day of acclimation, 6 bumblebee nests were randomly selected as 3 imidacloprid treatments and 3 control trials. Fresh sugar solution with or without imidacloprid and pollen were provided daily to the colony. The sugar solution was prepared from granulated sugar of sugar beets diluted in drinking water 1/1 (wt/wt). Drinking water was used because distilled water is harmful to organisms. The source of water used in the study was determined to be free of pesticides as determined by broad pesticide screening (data not shown). A stock imidacloprid solution was prepared by dilution of an analytical standard (Cat No. 37894, Sigma-Aldrich, St. Louis, MO, USA) in nanopure water (Thermo, Waltham, MA, USA). The stock solution was aliquoted and frozen, and a new tube was used for each daily application, which ensured that the same dose was used for the daily fresh treatment. The imidacloprid dose was based on studies showing that the imidacloprid content in field realistic doses is approximately a few μg per kg of pollen and nectar [1–3,5,6]. For the first week, we applied 0.1 μg of imidacloprid in 40 mL of the sugar solution, and the dose was then increased twofold. The experiment terminated on the 46th day after the beginning of the experiment by placing granulated dry ice in the box. The frozen colony was dismantled, and samples were collected. For the analysis in this study, we selected worker bumblebees. The sample for proteomics analysis consisted of heads that were cut from the body in the frozen state. Antennae were also removed. The remaining body was used for the pesticide analysis. Thus, we analyzed the same bumblebees for proteomics (heads) and pesticide content (remaining body). From each colony, two biological samples consisting of 10 individual heads or the rest of the bodies were prepared.

2.2. Sample processing

The head and body bumblebee samples were homogenized using a 5-mL or 50-mL Potter-Elvehjem tissue grinder (Kartell Labware division, Noviglio, Italy), respectively, powered by a driving force. The 10 heads were homogenized in 2 mL of 100 mM triethylammonium bicarbonate buffer (TEAB; Cat No. 17902, Fluka, Sigma-Aldrich) containing 2% sodium deoxycholate (SDC; Cat No. 30970, BioXtra, Sigma-Aldrich). Protein concentration was determined using BCA protein assay kit (Cat No. 23225, Thermo). Cysteines were reduced with 5 mM final concentration of TCEP (60 °C for 60 min) and blocked with 10 mM final concentration of MMTS (10 min room temperature). Samples were digested with trypsin (trypsin/protein ratio 1/20) at 37 °C overnight. Then, the samples were acidified with trifluoroacetic acid to final concentration of 1%. SDC was removed by extraction to ethylacetate [34], and afterwards to hexane. The peptides were desalted on Michrom C18 column. Dried peptides were resuspended in 25 μL of water containing 2% acetonitrile and 0.1% trifluoroacetic acid. The sample was further analyzed *via* nanoLC-MS/MS.

The bodies without heads were homogenized in an initial volume of 15 mL of nanopure water, and 10 mL was then used to rinse the rest of the homogenate into a 50-mL centrifuge tube (Orange Scientific). The homogenate was concentrated by lyophilization and stored at −80 °C until extraction and pesticide UHPLC-QqQ-MS/MS analysis.

2.3. UHPLC-MS/MS pesticide analysis

We aimed to analyze imidacloprid and its metabolites; however, the method also included a number of other pesticides. Standard solutions

of imidacloprid (CAS 138261-41-3), imidacloprid-olefin (CAS 115086-54-9), and imidacloprid-urea (CAS 120868-66-8) were obtained from Neochema (Bodenheim, Germany). The isotopically labeled standards used for calculations of the observed compounds were carbendazim-d4 and methamidophos-d6 purchased from Dr. Ehrenstorfer (Augsburg, Germany). LC-MS-grade acetonitrile (ACN) and LC-MS-grade methanol (MeOH), ammonium acetate (eluent additive for LC-MS), ammonium formate (for mass spectrometry, ≥ 99.0%), magnesium sulfate (reagent plus), sodium chloride (reagent plus), sodium citrate tribasic dehydrate (ASC reagent), sodium citrate dibasic sesquihydrate, Discovery DCS-18, and PSA SPE bulk sorbent were obtained from Sigma-Aldrich (St. Louis, MO, USA). The reagent-grade water used for sample processing and UHPLC-MS/MS was prepared using a Milli-Q system (Millipore, Darmstadt, Germany).

Before analysis, the lyophilized homogenized samples were left to stand at room temperature for 30 min. Isotopically labeled standards were added, and the sample was extracted using reagent-grade water, ACN and hexane. A combination of citrate QuEChERS salt [35] was added, immediately shaken and then centrifuged. Then, an aliquot of the ACN layer (under the hexane layer) was mixed with sorbents ($MgSO_4$, PSA and C18) for cleanup of the extract. The sample was shaken and centrifuged again. An aliquot of 3 mL of cleanup extract was evaporated to near dryness, further reconstituted in the mobile phase and filtered using 13-mm syringe filters into an autosampler vial.

UHPLC-MS/MS analysis was performed using an Acquity ultra-performance liquid chromatographic system (UHPLC, Waters, Milford, MA, USA) coupled with a Xevo TQ-S triple-quadrupole mass spectrometer (Waters). Chromatographic separation was performed on a BEH C18 analytical column (100 mm × 2.1 mm, 1.7 µm; Waters) protected by a VanGuard pre-column (5.0 mm × 2.1 mm, 1.7 µm; Waters). The column temperature was maintained at 40 °C throughout the analysis. The mobile phase consisted of 5 mM ammonium acetate and methanol at a flow rate of 0.4 mL/min using a gradient mode of elution. A volume of 5 µL of the sample was injected into the chromatographic system. The temperature of the autosampler was thermostated at 10 °C, and electrospray ionization was performed in positive mode. For each compound, two MRM transitions (Table S1) were used for quantitation and confirmation. The instrument was controlled using MassLynx software (v. 4.1; Waters), and data evaluation was performed using TargetLynx software (v. 4.1; Waters).

2.4. nanoLC-MS/MS proteomics analysis

All samples digested with trypsin were analyzed by nanoLC coupled with Orbitrap Fusion™ Tribrid™ mass spectrometry (nanoLC-MS/MS) in 2 analytical replicates in one analytical series; thus, 24 nanoLC-MS/MS runs were performed consecutively. Nano Reversed phase column (EASY-Spray column, 50 cm × 75 µm ID, PepMap C18, 2 µm particles, 100 Å pore size) was used for LC-MS/MS analysis. Mobile phase buffer A was composed of water and 0.1% formic acid. Mobile phase B was composed of acetonitrile and 0.1% formic acid. Samples were loaded onto the trap column (Acclaim PepMap300, C18, 5 µm, 300 Å Wide Pore, 300 µm × 5 mm) at a flow rate of 15 µL/min. Loading buffer was composed of water, 2% acetonitrile and 0.1% trifluoroacetic acid. Peptides were eluted with gradient of B from 4% to 35% over 60 min at a flow rate of 300 nL/min. Eluting peptide cations were converted to gas-phase ions by electrospray ionization and analyzed using the nLC-MS/MS. Survey scans of peptide precursors from 350 to 1400 *m/z* were performed at 120 K resolution (at 200 m/z) with a 5×10^5 ion count target. Tandem MS was performed by isolation at 1.5 Th with the quadrupole, HCD fragmentation with normalized collision energy of 30, and rapid scan MS analysis in the ion trap. The MS2 ion count target was set to 10^4 and the max injection time was 35 ms. Only those precursors with charge state 2–6 were sampled for MS^2. The dynamic exclusion duration was set to 45 s with a 10 ppm tolerance around the selected precursor and its isotopes. Monoisotopic precursor selection was turned on. The instrument was run in top speed mode with 2 s cycles [36,37].

The data were analyzed and quantified with label-free algorithms using MaxQuant software (version 1.5.3.8) [38] and Perseus (version 1.5.6.0) [39,40]. The FDR was set to 1% for both proteins and peptides, and we specified a minimum length of seven amino acids. The Andromeda search engine was used for the MS/MS spectra search against the *B. terrestris* database containing 20,931 records downloaded from NCBI on 21st February 2017. The enzyme specificity was set as C-terminal to Arg and Lys, allowing for cleavage at proline bonds and a maximum of two missed cleavages. MethylThio was selected as a fixed modification, and N-terminal protein acetylation and methionine oxidation were selected as variable modifications. The data were evaluated using a *t*-test in Perseus with a threshold *p*-value of 0.05.

2.5. Individual inspection of proteomics data

The proteins that changed significantly, that is, log2-fold change ≥0.3, were individually inspected in detail for gene ontology (GO) molecular function, GO biological process, function in UniProt and/or conserved domains (CCDs) [41]. Furthermore, we searched the proteins/enzymes individually in the Kyoto Encyclopedia of Genes and Genomes (KEGG) [42]. Finally, we found honeybee analogs to the bumblebee proteins/genes and searched them for the functional protein association network (STRING v 10.5) [43,44]. During the evaluation, we also included in our dataset proteins that constitute important members of the affected pathways and that are important markers just because they did not change (for example, NP_001267847.1 geranylgeranyl pyrophosphate synthase-like). The results of these analyses are provided with interactive links in the supplementary Excel file (Table S4). Significantly enriched KEGG pathways and representative images of the network were generated from the STRING analysis. This complex analysis facilitated identification of the pathways and key markers impacted by imidacloprid exposure.

2.6. In silico experiment

We checked the known protein sequence of bumblebee sterol regulatory element-binding protein cleavage-activating protein (SCAP; NCBI Accession: XP_003403180.1), and for modeling, we used the sterol-sensing domain (amino acids 294-442). Using blastp [45], we found one homologous pdb structure, 3JD8 [46,47]. The identified sequence had only one available analog, the Niemann-Pick C1 protein (3JD8), which has substantial homology to sterol-sensing domains [48]. Then, we aligned the bumblebee SCAP to the 3JD8 structure using ClustalX 2.0 [49]. The alignment was then used as an input for Modeller 9.19 software [50] for 3D structure prediction. The validity of the resulting models was checked using PROCHECK software (G-score) [51], and the model with the best valid score was chosen for further investigation. This model was optimized by running 10 steepest descent energy minimization steps followed by 10 conjugated gradient, 20 steepest descent, 10 conjugated gradient and finally 10 steepest descent steps (GROMOS 96 force-field [52]). The validity of the final model was again checked by Procheck [51]. We used this model for our docking experiments using the program AutoDock Vina [53]. The ligand structures were obtained from the ChemSpider database (https://www.chemspider.com, 29th of June 2018) and processed using Avogadro software [54]. The 2D ligand-protein interaction diagrams were generated using LigPlot+ [55].

3. Results and discussion

3.1. High proportion of the dangerous metabolite imidacloprid-olefin

Although a great deal has been written about the influence of neonicotinoids on pollinators, the overwhelming majority of recent studies neglect to mention the generation of dangerous pesticide

Table 1

The protein markers that changed significantly (*t*-test; $p < 0.05$) and those with changes (exposed_x-y_control) of log2-fold ≥ 0.3.

The key KEGG pathways are provided for the proteins, and the table clearly demonstrates that terpenoid backbone biosynthesis (bter00900) and the fatty acid metabolism (bter01212) were highly suppressed. Note that not all proteins are included in the KEGG pathways, and some participate in many pathways. Thus, for the full information, see Table S4. Legend for the most important KEGGs is provided below this table. Support for the affected pathways is additionally provided in Fig. 1 and Table 2, where the honeybee analogs of bumblebee genes were analyzed in STRING.

exposed_x-y_control	Key KEGG pathways				Protein ID (the first result is provided)
−5.85					> XP_012173574.1 PREDICTED: glucose dehydrogenase [FAD, quinone]-like
−5.50					> XP_012170360.1 PREDICTED: LOW QUALITY PROTEIN: fatty-acid amide hydrolase 2-like
−4.64					> XP_012174245.1 PREDICTED: uncharacterized protein LOC100649203 isoform X2
−4.16					> XP_003397894.2 PREDICTED: uncharacterized protein LOC100648681
−4.00					> XP_012172593.1 PREDICTED: ABC transporter G family member 23-like isoform X3
−3.86	bter04146				> XP_012173842.1 PREDICTED: putative fatty acyl-CoA reductase CG5065
−3.19	bter00900				> NP_001267835.1 farnesyl pyrophosphate synthase-like
−3.18					> XP_012175223.1 PREDICTED: phospholipase B1, membrane-associated-like
−3.14	bter00900				> XP_012176522.1 PREDICTED: 3-hydroxy-3-methylglutaryl-coenzyme A reductase
−3.07					> XP_003397876.1 PREDICTED: putative glycerol kinase 5
−2.59	bter00061	bter00071	bter01212		> XP_012176344.1 PREDICTED: very long-chain-fatty-acid–CoA ligase bubblegum isoform X2
−2.31					> XP_012169459.1 PREDICTED: cuticle protein 21-like
−2.29	bter00900	bter00072			> NP_001295236.1 hydroxymethylglutaryl-CoA synthase 1
−2.25					> XP_003398996.1 PREDICTED: esterase FE4-like isoform X1
−2.03					> XP_003402153.1 PREDICTED: insulin-like growth factor-binding protein complex acid labile subunit
−1.83	bter00900				> NP_001267865.1 diphosphomevalonate decarboxylase
−1.76					> XP_003398464.1 PREDICTED: sensory neuron membrane protein 1 isoform X2
−1.73	bter00561				> XP_012163583.1 PREDICTED: 2-acylglycerol O-acyltransferase 1-like isoform X1
−1.70	bter00062	bter01040	bter01212		> XP_003402957.1 PREDICTED: very-long-chain 3-oxoacyl-CoA reductase-like
−1.67	bter00480	bter00980	bter00982		> XP_003402656.1 PREDICTED: microsomal glutathione S-transferase 1-like
−1.65	bter00900	bter04146			> NP_001267845.1 phosphomevalonate kinase
−1.51	bter00900				> NP_001267855.1 isopentenyl-diphosphate Delta-isomerase 1-like
−1.41					> XP_012174983.1 PREDICTED: LOW QUALITY PROTEIN: uncharacterized protein LOC100645665
−1.41					> XP_003399213.1 PREDICTED: venom dipeptidyl peptidase 4
−1.20					> XP_012166978.1 PREDICTED: protein yellow
−1.18					> XP_012167590.1 PREDICTED: juvenile hormone epoxide hydrolase 1-like
−1.12					> XP_012165799.1 PREDICTED: glutaminyl-peptide cyclotransferase isoform X1
−1.12					> XP_012168894.1 PREDICTED: uncharacterized protein LOC100645018
−1.04					> XP_012172430.1 PREDICTED: ABC transporter G family member 20 isoform X2
−1.00					> XP_012176575.1 PREDICTED: transmembrane protein 120 homolog isoform X1
−0.96	bter00900	bter04146			> XP_012169516.1 PREDICTED: mevalonate kinase isoform X1
−0.96					> XP_012167920.1 PREDICTED: uncharacterized protein LOC100643536 (protein javelin)
−0.95					> XP_003399181.1 PREDICTED: alpha-tocopherol transfer protein-like
−0.91					> XP_003401255.1 PREDICTED: cysteine-rich venom protein 6-like
−0.86	bter00061	bter01212			> XP_012170551.1 PREDICTED: acetyl-CoA carboxylase isoform X3
−0.79	bter00480				> XP_003395542.1 PREDICTED: probable phospholipid hydroperoxide glutathione peroxidase
−0.70					> XP_003397806.1 PREDICTED: cytochrome *b*5-like
−0.70	bter01040	bter01212			> NP_001267818.1 acyl-CoA delta-9 desaturase
−0.65	bter04146	bter00061	bter00071	bter01212	> XP_003397572.1 PREDICTED: long-chain-fatty-acid–CoA ligase 4 isoform X3
−0.62					> XP_012167050.1 PREDICTED: fibroin heavy chain-like
−0.61					> XP_012165031.1 PREDICTED: regulator of microtubule dynamics protein 1-like isoform X2
−0.61					> XP_012168727.1 PREDICTED: alpha-tocopherol transfer protein-like isoform X1
−0.57					> XP_003398056.1 PREDICTED: DNA-directed RNA polymerase II subunit RPB1-like
−0.57	bter04141				> XP_012173329.1 PREDICTED: ero1-like protein isoform X2
−0.56					> XP_012163493.1 PREDICTED: acyl-CoA dehydrogenase family member 9, mitochondrial
−0.56	bter00030	bter01200	bter01230		> XP_012165021.1 PREDICTED: transaldolase
−0.55					> XP_003403296.2 PREDICTED: uncharacterized protein LOC100646399
−0.55					> XP_003398432.1 PREDICTED: pancreatic lipase-related protein 2-like
−0.54					> XP_012168044.1 PREDICTED: 15-hydroxyprostaglandin dehydrogenase [NAD(+)]-like
−0.53	bter00620	bter01200			> XP_003401441.1 PREDICTED: NADP-dependent malic enzyme isoform X2
−0.53					> XP_003398801.1 PREDICTED: acyl-CoA-binding protein homolog
−0.51					> XP_003397010.1 PREDICTED: ER membrane protein complex subunit 10
−0.50					> XP_012176035.1 PREDICTED: dehydrogenase/reductase SDR family protein 7-like
−0.50	bter00071	bter01212			> XP_003397432.1 PREDICTED: very long-chain specific acyl-CoA dehydrogenase, mitochondrial
−0.49					> XP_012169017.1 PREDICTED: elongation factor Ts, mitochondrial
−0.49					> XP_003403408.2 PREDICTED: alcohol dehydrogenase-like, partial
−0.48					> XP_003396495.1 PREDICTED: ejaculatory bulb-specific protein 3
−0.47	bter00561	bter00564			> XP_003395337.1 PREDICTED: 1-acyl-sn-glycerol-3-phosphate acyltransferase gamma-like
−0.47	bter00061	bter01212			> NP_001267840.1 fatty acid synthase-like
−0.46	bter00280				> XP_003399167.1 PREDICTED: LOW QUALITY PROTEIN: methylglutaconyl-CoA hydratase, mitochondrial
−0.45					> XP_012165439.1 PREDICTED: nudix hydrolase 8
−0.45					> XP_003402252.1 PREDICTED: ER membrane protein complex subunit 4
−0.43	bter00062	bter01040	bter01212		> XP_003395506.1 PREDICTED: very-long-chain enoyl-CoA reductase
−0.43					> XP_003399739.1 PREDICTED: venom carboxylesterase-6
−0.42					> XP_003393753.1 PREDICTED: putative tricarboxylate transport protein, mitochondrial
−0.41					> XP_003402810.1 PREDICTED: mitochondrial dicarboxylate carrier
−0.41					> XP_012175822.1 PREDICTED: LOW QUALITY PROTEIN: fatty-acid amide hydrolase 2
−0.41	bter00900	bter00981			> XP_003401519.1 PREDICTED: dehydrogenase/reductase SDR family member 11-like
−0.39					> XP_012174181.1 PREDICTED: ATP-binding cassette sub-family G member 1 isoform X1

(*continued on next page*)

Table 1 (*continued*)

exposed_x-y_control	Key KEGG pathways				Protein ID (the first result is provided)
−0.39	bter00900	bter00071	bter00072	bter01212	> NP_001267862.1 acetyl-CoA acetyltransferase
−0.38	bter00052	bter00500			> XP_012164669.1 PREDICTED: alpha-glucosidase-like
−0.37					> XP_012167652.1 PREDICTED: circadian clock-controlled protein-like
−0.36	bter00020				> XP_012171737.1 PREDICTED: ATP-citrate synthase
−0.35	bter00564	bter04142			> XP_003393035.1 PREDICTED: group XV phospholipase A2-like [*Bombus terrestris*] (lysophospholipase III)
−0.35	bter00480	bter00980	bter00982	bter00983	> XP_012172050.1 PREDICTED: uncharacterized protein LOC100646009 (GSTD1)
−0.35					> XP_012173981.1 PREDICTED: LOW QUALITY PROTEIN: 28S ribosomal protein S27, mitochondrial
−0.34	bter00062	bter00071	bter01212	bter01040	> XP_003398896.1 PREDICTED: trifunctional enzyme subunit alpha, mitochondrial
−0.32	bter00830	bter04146			> XP_003398346.1 PREDICTED: dehydrogenase/reductase SDR family member 4
−0.31					> XP_012167473.1 PREDICTED: calcineurin B homologous protein 1
−0.31					> XP_003393818.1 PREDICTED: myelin P2 protein isoform X1
−0.31					> XP_012170200.1 PREDICTED: probable pterin-4-alpha-carbinolamine dehydratase
−0.30	bter00062	bter00071	bter01212		> XP_003394912.1 PREDICTED: trifunctional enzyme subunit beta, mitochondrial (acetyl-CoA acyltransferase)
−0.30					> XP_003398947.1 PREDICTED: transmembrane protein 177
−0.30	bter00071	bter01212			> XP_012173761.1 PREDICTED: carnitine O-palmitoyltransferase 1, liver isoform isoform X2
0.30					> XP_012164143.1 PREDICTED: titin-like isoform X1
0.30					> XP_003402977.1 PREDICTED: alpha-crystallin B chain isoform X1
0.31					> XP_012176738.1 PREDICTED: uncharacterized protein LOC100651154 isoform X1
0.34	bter00040	bter00051			> XP_012174783.1 PREDICTED: sorbitol dehydrogenase-like isoform X2
0.34					> XP_012172948.1 PREDICTED: muscle-specific protein 20
0.37					> XP_012168003.1 PREDICTED: uncharacterized protein LOC100650291 isoform X3
0.37					> XP_003395464.1 PREDICTED: muscle M-line assembly protein unc-89 isoform X2
0.38					> XP_012169760.1 PREDICTED: alpha-actinin, sarcomeric isoform X1
0.38					> XP_012169471.1 PREDICTED: uncharacterized protein LOC100649546 isoform X3
0.39					> XP_012166945.1 PREDICTED: probable phosphorylase b kinase regulatory subunit beta isoform X2
0.41					> XP_003402554.1 PREDICTED: alpha/beta hydrolase domain-containing protein 11 isoform X1
0.42	bter00740				> XP_012168140.1 PREDICTED: LOW QUALITY PROTEIN: riboflavin kinase
0.47					> XP_012170960.1 PREDICTED: neocalmodulin-like isoform X4
0.47					> XP_003399704.1 PREDICTED: protein CREG1
0.49	bter00190				> XP_012174161.1 PREDICTED: uncharacterized protein LOC100647597
0.54	bter04141	bter04213			> XP_012170000.1 PREDICTED: protein lethal(2)essential for life-like
0.61	bter04144				> XP_003395422.1 PREDICTED: IST1 homolog
0.67					> ALO64437.1 ATP synthase F0 subunit 6 (mitochondrion)
1.05					> XP_003401642.1 PREDICTED: cuticle protein 18.7-like (lamprin)
1.11					> XP_012171341.1 PREDICTED: filamin-A isoform X5
1.27					> XP_012169553.1 PREDICTED: troponin C, isoform 3 isoform X2

KEGGs: bter00061, Fatty acid biosynthesis; bter00072, Synthesis and degradation of ketone bodies; bter00900, Terpenoid backbone biosynthesis; bter00071, Fatty acid degradation; bter00561, Glycerolipid metabolism; bter04146, Peroxisome; bter00062, Fatty acid elongation; bter00564, Glycerophospholipid metabolism; bter01212, Fatty acid metabolism; bter01040, Biosynthesis of unsaturated fatty acids; bter00981, Insect hormone biosynthesis

metabolites. Research performed close to the end of the 20th or beginning of the 21st century showed that imidacloprid-olefin can be 10-fold more toxic to insects than imidacloprid [56–58]. This possibility of forming a more effective compound than the parent compound not only makes imidacloprid a potentially more effective agent against target insect pests but also represents a hidden danger to nontarget organisms. In an important finding, Suchail et al. [12] showed that imidacloprid-olefin is 2 times more toxic to honeybees than imidacloprid [12]. In another study, Suchail et al. [59] showed that imidacloprid-olefin preferentially occurred in the head, thorax and abdomen. Recently [11], we demonstrated the formation of imidacloprid-olefin in green plant tissues. Thus, due to the importance of the imidacloprid-olefin metabolite, we verified its presence in our experiment in addition to imidacloprid. To determine the extent of imidacloprid metabolic transformation in bumblebees through another important detoxification pathway [59], we also measured imidacloprid-urea, which has been shown to be less toxic to bees [12]. We used bumblebee heads for the proteomic analysis and the rest of the same bodies for the pesticide/pesticide-metabolite analysis. The analytes were quantified using UHPLC-QqQ-MS/MS, and for the key observed compounds, two MRM transitions and internal standards (ISTDs) (Table S1) were used for quantitation and confirmation. The results in Table S2 show that only imidacloprid and imidacloprid-olefin were detected in quantities of 0.57 ± 0.22 and 1.95 ± 0.43 ng/g, respectively. Moreover, the imidacloprid-urea metabolite was not detected. Thus, our findings in bumblebees are consistent with previous reports that imidacloprid-olefin is one of the metabolites that is formed relatively quickly in honeybees [59–61]. However, most importantly, our analysis revealed that the levels of imidacloprid-olefin were 3.4-fold higher than those of imidacloprid in the investigated samples. Thus, bumblebee metabolism maintains a high proportion of the dangerous metabolite imidacloprid-olefin. Considering the sum of both of these molecules, there was *ca.* 0.6 ng of active substance per bumblebee compared with 0.14 ng measured when only imidacloprid was analyzed. From a methodical point of view, all studies that detect only imidacloprid overlook the additional amount of imidacloprid-olefin. Finally, the formation of the imidacloprid-olefin metabolite and its persistence at a relatively high rate compared with the parent compound can explain the delayed and cumulative effects of imidacloprid exposure [14,15].

3.2. Suppression of the entire mevalonate pathway and fatty acid synthesis

To ascertain the impact of sublethal imidacloprid exposure on bumblebee physiology at the molecular level, we analyzed bumblebee worker heads using a label-free quantitative proteomics approach employing a state-of-the-art nanoLC coupled with an Orbitrap Fusion™ Tribrid™ mass spectrometer. Consecutive analysis of 24 nanoLC-MS/MS runs enabled quantitative comparison of 2883 proteins (Table S3). Imidacloprid exposure significantly (*t*-test; $p < 0.05$) influenced the abundance of 206 proteins (Table S3 and S4), and proteins that showed a log2-fold change ≥0.3 (Table 1 and S4) were individually inspected in detail in different databases and with bioinformatics tools. The results of these analyses with interactive links are provided in Table S4. This complex and detailed analysis facilitated the identification of the

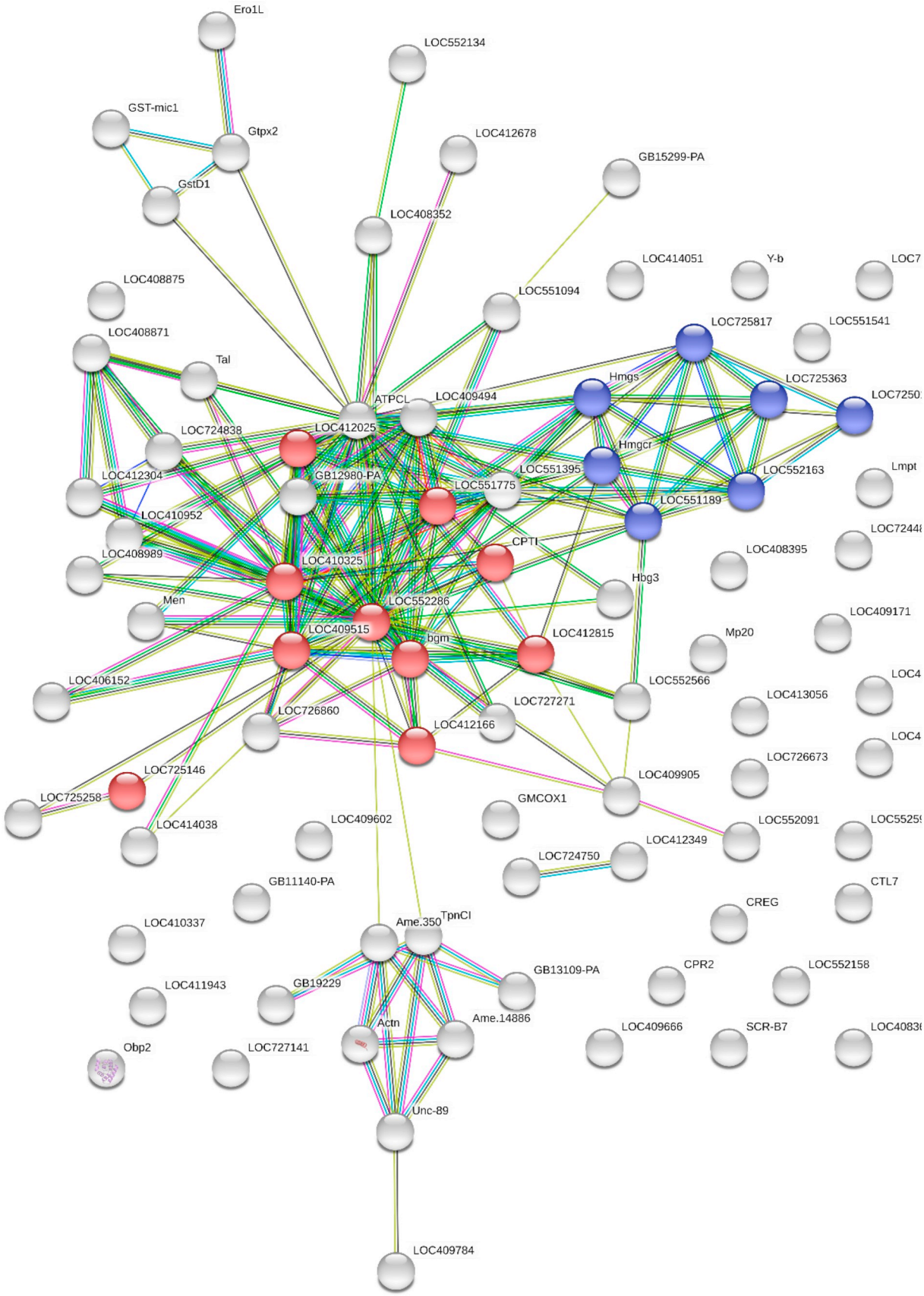

Fig. 1. The two most important KEGG pathways are highlighted (see also Table 2) in the STRING network generated from the honeybee analogs of bumblebee genes. Fatty acid metabolism nodes are in red, while terpenoid backbone biosynthesis nodes are in blue. In the network, we can also see how the markers are interconnected and that some have many partners. Thus, for instance, downregulation of CAA (here LOC552286) and ATPCL should have variable and extensive consequences. (For interpretation of the references to colour in this figure legend, the reader is referred to the web version of this article.)

Table 2
STRING analysis of honeybee analogs of bumblebee genes.

#Pathway ID	Pathway description	Observed gene count	False discovery rate
01212	Fatty acid metabolism	10	2.00E-12
00900	Terpenoid backbone biosynthesis	7	1.85E-09
01100	Metabolic pathways	23	8.41E-09
00071	Fatty acid degradation	6	6.21E-07
01040	Biosynthesis of unsaturated fatty acids	3	0.00102
00062	Fatty acid elongation	3	0.00121
00280	Valine, leucine and isoleucine degradation	4	0.00122
04146	Peroxisome	4	0.00537
00061	Fatty acid biosynthesis	2	0.00888
00480	Glutathione metabolism	3	0.0113
00980	Metabolism of xenobiotics by cytochrome P450	2	0.0184
00982	Drug metabolism - cytochrome P450	2	0.0184
00650	Butanoate metabolism	2	0.0328
01120	Microbial metabolism in diverse environments	4	0.0411

The STRING network analysis which provided 85 nodes and 178 edges, is the result of the analysis of honeybee gene analogs (source: column "STRING *Apis mellifera*" in Table S4). Overall, 14 KEGG pathways were significantly enriched in the network, and the protein nodes of the fatty acid metabolism (in red) and terpenoid backbone biosynthesis (in blue) pathways are also highlighted in Fig. 1.

key pathways, markers and connections impacted by imidacloprid exposure.

Our analyses of the proteomics results (Fig. 1, Tables 1, 2 and S4) indicated that a number of the highly downregulated markers are members of the terpenoid backbone biosynthesis pathway (KEGG: bter00900). While investigating the changes more specifically, we recognized that there all markers that belonging to the mevalonate or isoprenoid pathway (Fig. 2), which produces isopentenyl pyrophosphate (isopentenyl-PP) or dimethylallyl pyrophosphate (dimethylallyl-PP) as end products from acetyl-CoA, were significantly downregulated. Moreover, farnesyl pyrophosphate synthase (EC: 2.5.1.10), which produces the key C10-C20 isoprenoid (2E, 6E)-farnesyl-PP, was also strongly downregulated. Interestingly, as shown in Fig. 2, subsequent enzymes processing (2E, 6E)-farnesyl-PP did not quantitatively change. Furthermore, we identified important downregulation of other pathways (Fig. 1, Tables 1, 2 and S4), most importantly in fatty acid metabolism (KEGG: bter01212), degradation (KEGG: bter00071), and elongation (KEGG: bter00062); biosynthesis of unsaturated fatty acids (bter01040); glycerolipid metabolism (bter00561); peroxisome (bter04146); and synthesis and degradation of ketone bodies (bter00072). Thus, Fig. 2 also shows key pathways/markers directly connected to the mevalonate pathway suppression and that the next downregulated pathway was fatty acid biosynthesis (KEGG: bter00061); the key downregulated enzymes of fatty acid biosynthesis were acetyl-CoA carboxylase (CAA; EC: 6.4.1.2) [62] and fatty acid synthase (FAS; EC: 2.3.1.85).

The mevalonate and fatty acid synthesis pathways are essential for any organism and therefore are tightly regulated. Hydroxymethylglutaryl-CoA reductase (Hgmcr; EC: 1.1.1.34) and CAA are the rate-limiting enzymes of the mevalonate [63,64] and fatty acid synthesis pathways [62,65], respectively. Hgmcr belongs to a group of highly regulated enzymes, and several feedback mechanisms exist [63]; for instance, the inhibition of Hgmcr by statins is pharmaceutically utilized to decrease cholesterol levels [64]. Additionally, CAA is a popular although intractable drug target [65]. It is clear that such a combined effect that consecutively downregulates the entire mevalonate pathway and CAA should have a single origin. Contemplating the mechanism brought us to an attractive candidate, sterol regulatory element-binding proteins (SREBPs), which are well-known transcription factors for (i) the entire mevalonate pathway [66], (ii) CAA and FAS (Fig. 2) [67], and (iii) other downregulated proteins related to the synthesis of cholesterol, fatty acids, triacylglycerols and phospholipids (see the KEGGs in Table 1 and S4) [67]. For instance, downregulated acyl-CoA delta-9 desaturase or stearoyl-CoA desaturase (SCD1; EC: 1.14.19.1) is one of the key additional involved markers [67–69]. Notably, unlike vertebrates, insects are not capable of *de novo* synthesis of sterol compounds. Thus, they depend on dietary sterols [70]; however and importantly, insects are endowed with all known components of the SREBP pathway [71]. The key activating component of the SREBP pathway is SCAP, which controls the proteolytic cleavage of the SREBP precursor to form particular transcription factors [71,72]. Thus, we suggest that the mechanism of imidacloprid involves SCAP blockade, which hinders the generation of transcriptionally active SREBP isoforms.

To verify our suggestion that imidacloprid binds SCAP, we conducted an *in silico* experiment in which cholesterol, imidacloprid and its metabolites were docked with SCAP. The resulting interaction energies in the docking experiment (Table 3) indicated that all tested molecules, *i.e.*, imidacloprid, imidacloprid-olefin, 5-hydroxy imidacloprid and desnitro-imidacloprid, have higher affinity to the SCAP receptor than cholesterol. To demonstrate the ligand-SCAP interactions, we provide the 2D ligand-protein interaction diagrams (Fig. 3a–e) and 3D visualization (Fig. 4ab). The possibility that the tested ligands block SCAP from sensing sterols and regulating sterol synthesis [71,72] indicates a novel toxicogenic action of imidacloprid and its metabolites. The toxicogenic effect is highlighted by the affinity of the metabolites for SCAP, mainly imidacloprid-olefin (Fig. 3c), which we found in bumblebees in a substantially higher proportion than imidacloprid.

3.3. The complex consequences of imidacloprid exposure

The neonicotinoids were developed to bind to the nicotinic acetylcholine receptor (nAChR) of invertebrate pests. However, the different neonicotinoids bind differently to nAChR [73]. Furthermore, interestingly, desnitro-imidacloprid has previously been shown to interact with α4β2-nAChR in the mammalian brain [74], which is involved in learning [75]. As reported above, desnitro-imidacloprid can also bind SCAP (Fig. 3e). Although nAChR subunit diversity varies among insects and mammals [76], learning and memory are believed to be affected by nAChR in bees as well [19,77]. The effect of the well-known affinity of imidacloprid for nAChRs correspond to the downregulated esterase FE4-like (cholinesterase 1-like); for instance, imidacloprid suppresses acetylcholinesterase (AChE) activity in *Chironomus riparius* larvae, and the authors linked the reduced AChE activity to behavior [78]. Furthermore, the notable downregulation of ATP-citrate synthase (ATPCL; EC: 2.3.3.8) is included in the schema in Fig. 2; in addition to its role in acetyl-CoA synthesis, ATPCL is involved in acetylcholine biosynthesis in the brain [79]. Note that the STRING network (Fig. 1) illustrates that an effect on ATPCL could impact many genes, and the effect of ATPCL downregulation should be therefore very complex.

The effects connected with nAChR are not surprising, but we found a novel toxicogenic mechanism of the effect of imidacloprid. The disruption of the mevalonate pathway alone is a strong indicator of

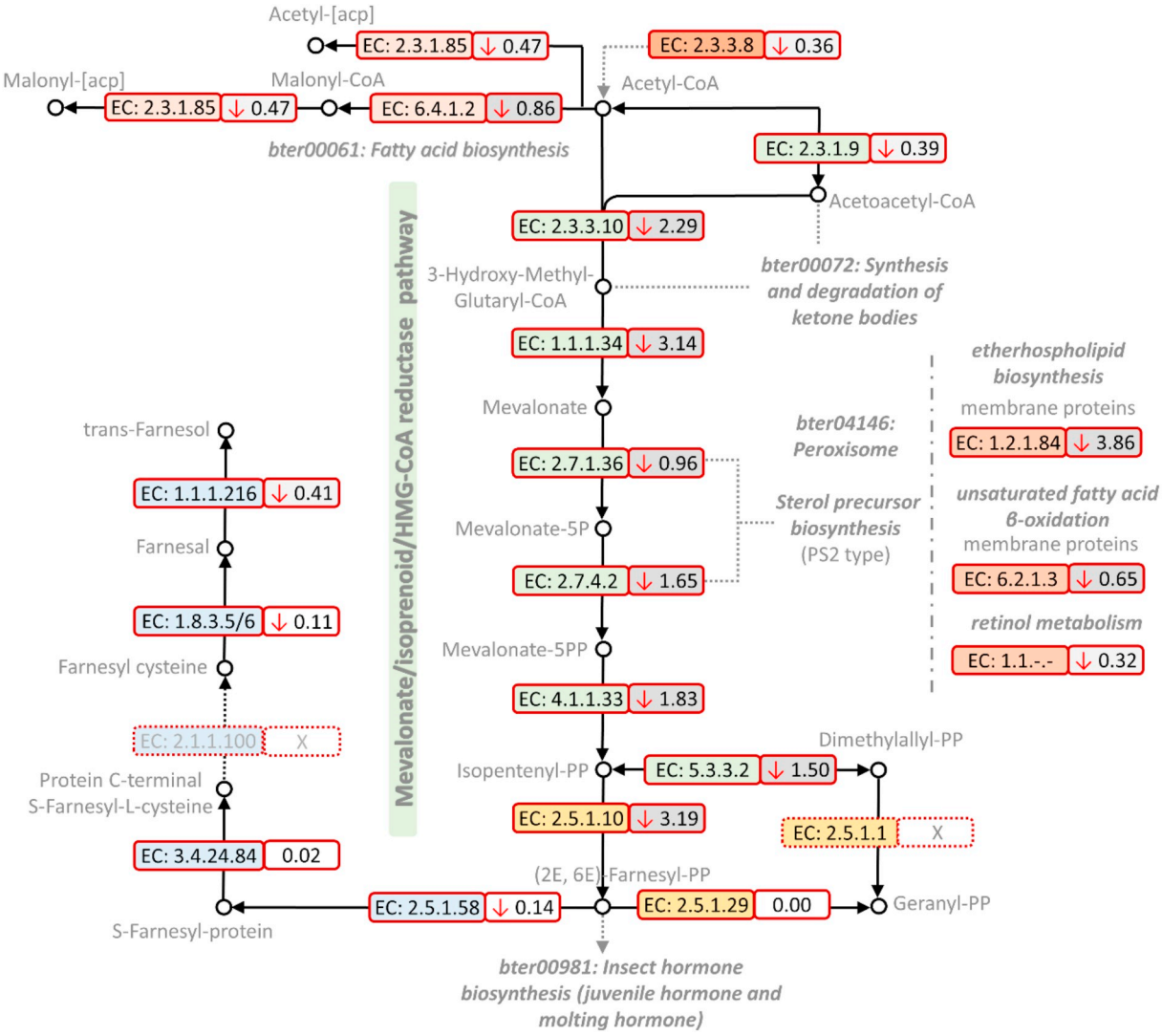

Fig. 2. Schematic presentation demonstrating suppression of the entire mevalonate pathway and fatty acid synthesis. As shown in the chart, mevalonate pathway suppression is directly connected to the synthesis of ketone bodies, peroxisomes and hormones. Additionally, from the two enzymes of the mevalonate pathway MVK (EC:2.7.1.36) and PMVK (EC:2.7.4.2), which are members of the peroxisomal pathway regulating sterol precursor synthesis (PS2 type), we found downregulated peroxisomal enzymes associated with membrane protein genesis and retinol metabolism. Another important downregulated enzyme, ATPCL, synthesizes acetyl-CoA and is consequently involved in acetylcholine biosynthesis in the brain. However, it is evident that most of the changes shown in this schema are not due to blockade of the neonicotinic acetylcholine receptor. Instead, imidacloprid has another target discovered in this study, SCAP. Legend: EC – Enzyme Commission number; the number in the small frame means log2-fold change; ↓ – the marker was downregulated; X – the marker was not found in the dataset containing 2883 proteins in Table S3.

Table 3
Interaction energy results from the molecular docking experiment. Cholesterol, imidacloprid, imidacloprid-olefin, 5-hydroxy imidacloprid and desnitro-imidacloprid were docked with the SCAP structure. The resulting energies clearly indicate that imidacloprid and its metabolites have higher affinity for SCAP than the prototype molecule cholesterol. The highest affinity was found for the dangerous and, in our study, high-abundance metabolite imidacloprid-olefin.

Bumblebee SCAP receptor (model)	
Molecule	Energy [kcal/mol]
Cholesterol	−5.5
Imidacloprid	−6.7
Imidacloprid-olefin	−6.8
5-Hydroxy imidacloprid	−6.2
Desnitro-imidacloprid	−6.4

multiple disease signs, including neurological abnormalities [80,81]. The complex adverse effects related to suppression of the mevalonate pathway also include impaired peroxisome function, synthesis and degradation of ketone bodies, and insect hormone biosynthesis (Fig. 2; Table 1). The impaired function of peroxisomal proteins reflects (i) disrupted sterol precursor biosynthesis (PTS2 type) by downregulated mevalonate kinase (MVK; EC:2.7.1.36) and phosphomevalonate kinase (PMVK; EC:2.7.4.2) of the mevalonate pathway; (ii) disrupted breakdown of long-chain fatty acids important for membrane protein genesis by downregulated putative fatty acyl-CoA reductase CG5065 (FAR; EC:1.2.1.84) and long-chain-fatty-acid—CoA ligase 4 (ACSL4; EC: 6.2.1.3), and (iii) suppressed retinol metabolism by downregulated dehydrogenase/reductase SDR family member 4 (DHRS4; EC:1.1.-.-). Furthermore, downregulated SCD1 is associated with alterations in the composition of long-chain fatty acids [69]. It is clear that these diverse marker changes, including downregulation of CAA and FAS, have a common cause in inactive SREBPs [67–69,71,82,83] through the blockade of SCAP by imidacloprid reported here.

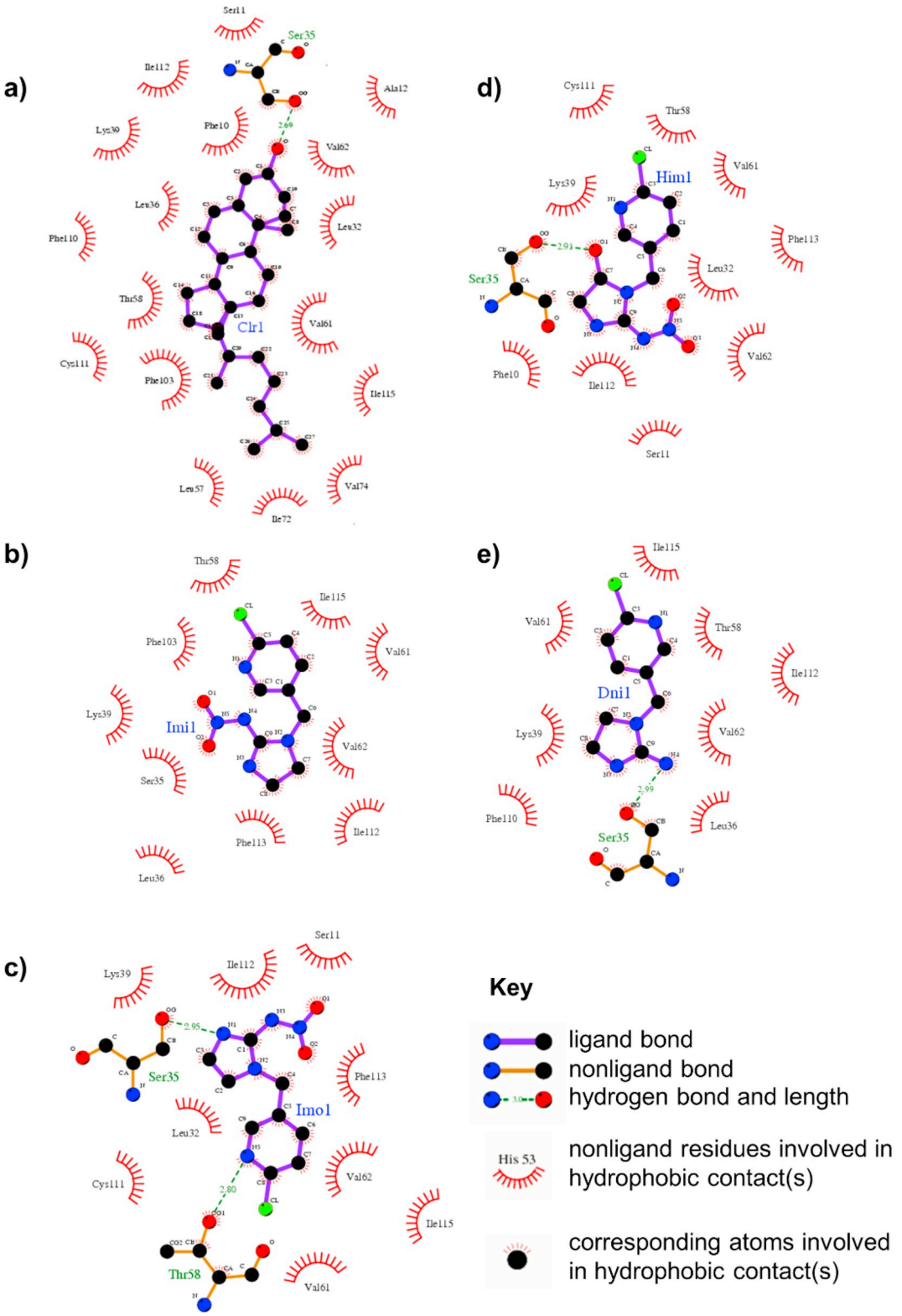

Fig. 3. *2D* ligand-protein interaction (Ligplot+) diagrams of the bumblebee SCAP sterol-sensing domain interacting with docked molecules. (a) cholesterol, (b) imidacloprid, (c) imidacloprid-olefin, (d) 5-hydroxy imidacloprid, and (e) desnitro-imidacloprid. The hydrophobic interactions of all docked compounds with residues Val[61], Val[62] and Ile[112] are clearly evident and effectively prevent cholesterol binding.

Furthermore, we suggest that disruption of lipid homeostasis influences bumblebee communication [84]. We stress the substantial downregulation of neuron membrane protein 1 (Snmp1), which is important in olfaction and sensitivity to pheromones. In *Drosophila*, Snmp1 has been described as a receptor detecting the fatty-acid-derived male pheromone 11-cis vaccenyl acetate (cVA) [85,86]. Importantly, in relation to SREBPs [67–69], downregulated SCD1 should participate in the formation of pheromone precursors [87,88]. The disruption of

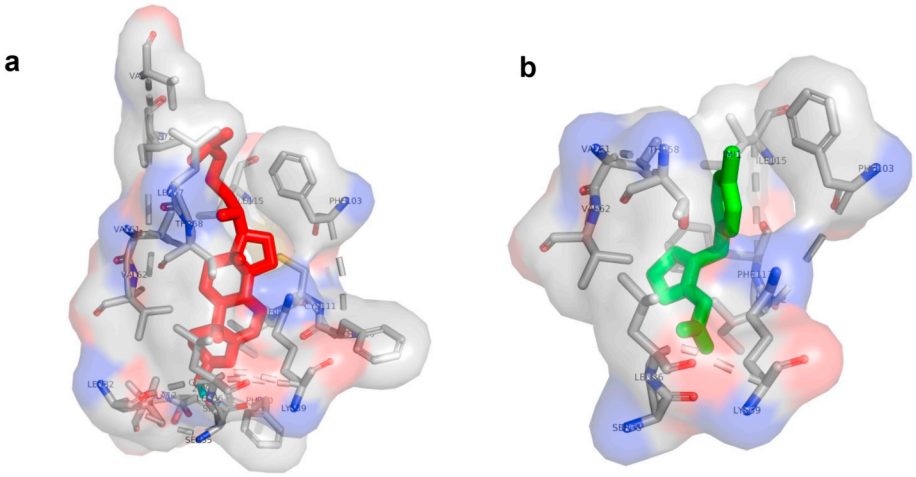

Fig. 4. The 3D structure of the bumblebee SCAP receptor with docked cholesterol (a) and imidacloprid (b). The cholesterol molecule is colored in red, while imidacloprid is colored in green. (For interpretation of the references to colour in this figure legend, the reader is referred to the web version of this article.)

olfaction is also indicated by the substantial downregulation (4th highest) of the uncharacterized protein LOC100648681, which is an analog of Obp2 in honeybees (Table S4). Changes in these markers indicate a violation of communication in the colony and can explain the previously reported adverse effects of imidacloprid on olfactory learning [17,18].

We do not have exact information about the most substantially downregulated enzyme in our study, glucose dehydrogenase [FAD, quinone]-like (EC:1.1.3.49); however, according to CCD, it belongs to the choline dehydrogenase and glucose-methanol-choline oxidoreductase (GMCOX) family and thus may participate in choline metabolism [89] and/or conversion of (*R*)-mandelonitrile to benzoyl cyanide [90]. In the context of the present study, it appears important that the GMCOX C-terminal domain is involved in steroid binding [91,92], and thus the reduced abundance of this protein is potentially connected to impaired sterol synthesis. The second most downregulated protein in our dataset was fatty-acid amide hydrolase 2-like (FAAH2), and two additional isoforms of FAAH2 were significantly downregulated (Table 1 and S4). FAAH2 hydrolyzes oleamide and anandamide, fatty acid amides that are involved in neurobehavioral processes such as sleep, pain, feeding, and memory [93]. Thus, we can hypothetically link downregulation of FAAH2 to commonly reported symptoms of neonicotinoid exposure. However, it is important to note that insects lack cannabinoid receptors (CB1 and CB2), and consequently, anandamide production is erased; however, the insects still synthesize another ligand, sn-2 arachidonoyl glycerol (2-AG), which is a known agonist for the absent receptors [94,95]. Certainly, in the future, it will be necessary to measure endocannabinoids in relation to imidacloprid-treated bees. In that context, showing the link between disrupted sterol and fatty acid synthesis and the proteins connected with arachidonic acid metabolism should be of interest (Table S4) because the arachidonic acid pathway participates in the regulation of cholesterol metabolism [96]. Finally, because oleamide is an oleic acid derivative, it is notable that downregulation of SCD1 should result in a decrease in oleic acid concentration and an accumulation of triacylglycerol [69].

Up to this point, we have discussed only proteins that were downregulated. Although the levels of upregulation were not as substantial on the log2-fold change scale, these changes also provide important information. One interesting feature is that the two most upregulated proteins were actin binding troponin C and filamin-A; some other muscle-type proteins and cuticle protein 18.7-like were also increased. These changes may reflect partial compensation for the disrupted synthetic pathways, such as the generation of membrane proteins. The fourth highest change we found was for the regulator of normal mitochondrial function synthase F0 subunit 6 (mitochondrial) (MT-ATP6). Fitting to our story, in medicine, mutations in MT-ATP6 are connected to neuropathy and ataxia [97], which correspond well to the described general adverse effects of imidacloprid on bees. Finally, we detected upregulation of small heat-shock proteins—protein lethal(2)essential for life-like (lethal(2)) and alpha-crystallin B chain. Importantly, overexpression of alpha-B crystallin has been observed in many neurological diseases [98], and according to KEGG, lethal(2) is a member of the longevity regulating pathway (bter04213).

3.4. Conclusion

We found that in bumblebees chronically exposed to sublethal field realistic dose of imidacloprid, the entire mevalonate pathway is strongly affected. Moreover, we observed suppression of fatty acid synthesis, generation of membrane proteins, function of fatty acid amide hydrolases 2 and disruption of olfaction. The upregulated proteins are consistent with these changes and suggest at least partial compensation for the disruption of sterol metabolism, which is vital for membranes. These changes are more obvious than those connected to the blockade of nAChR, which is the original target of neonicotinoids. Moreover, the affected markers and *in silico* experiment suggest that imidacloprid and its metabolites affect the function of SREBPs through SCAP blockade. Additional studies are necessary to show whether the effects of other neonicotinoids are similar to those of imidacloprid.

Competing interests

The authors declare no competing interests.

Author contributions

T.E. wrote the main manuscript. T.E., B.S., T.H., K.R., and A.P. designed the experiments. B.S. performed the *in silico* experiment and prepared related images. P.T. and K.H. performed the nanoLC-MS/MS analysis and evaluated the data. K.K. and T.E. contributed to the methodology of sample processing for analyses. T.E. evaluated the proteomics data, evaluated the proteome changes, and prepared the tables and figures.

Availability of data

The accession number for the Raw nanoLC-MS/MS runs reported in this paper is MassIVE MSV000082977.

Acknowledgments

This study was supported by Grant Nos. TA04020267, LD15028 and RO0418 of the Technology Agency of the Czech Republic, the Ministry of Education, Youth and Sports of the Czech Republic, and the Ministry of Agriculture of the Czech Republic, respectively. Computational resources were provided by the CESNETLM2015042 and the CERIT Scientific Cloud LM2015085, provided under the programme "Projects of Large Research, Development, and Innovations Infrastructures". We thank Marcela Seifrtova, Julie Chalupnikova, and Martin Markovic for valuable help.

Appendix A. Supplementary data

Supplementary data to this article can be found online at https://doi.org/10.1016/j.jprot.2018.12.022.

References

[1] J.M. Bonmatin, P.A. Marchand, J.F. Cotte, A. Aajoud, H. Casabianca, G. Goutailler, M. Courtiade, Bees and systemic insecticides (imidacloprid, fipronil) in pollen: Subnano-quantification by HPLC/MS/MS and GC/MS, in: A.A.M. Del Re, E. Capri, G. Fragoulis, M. Trevisan (Eds.), Environmental Fate and Ecological Effects of Pesticides, La Goliardica Pavese, Pavia, 2007, pp. 837–845.

[2] J.M. Bonmatin, I. Moineau, R. Charvet, C. Fleche, M.E. Colin, E.R. Bengsch, A LC/APCI-MS/MS method for analysis of imidacloprid in soils, in plants, and in pollens, Anal. Chem. 75 (2003) 2027–2033.

[3] A. Rortais, G. Arnold, M.-P. Halm, F. Touffet-Briens, Modes of honeybees exposure to systemic insecticides: estimated amounts of contaminated pollen and nectar consumed by different categories of bees, Apidologie 36 (2005) 71–83.

[4] V.A. Krischik, A.L. Landmark, G.E. Heimpel, Soil-applied imidacloprid is translocated to nectar and kills nectar-feeding *Anagyrus pseudococci* (Girault) (Hymenoptera: Encyrtidae), Environ. Entomol. 36 (2007) 1238–1245.

[5] G.P. Dively, A. Kamel, Insecticide residues in pollen and nectar of a cucurbit crop and their potential exposure to pollinators, J. Agric. Food Chem. 60 (2012) 4449–4456.

[6] J.M. Bonmatin, P.A. Marchand, R. Charvet, I. Moineau, E.R. Bengsch, M.E. Colin, Quantification of imidacloprid uptake in maize crops, J. Agric. Food Chem. 53 (2005) 5336–5341.

[7] European Commission (EC), Commission Implementing Regulation (EU) No 485/2013 of 24 May 2013 amending Implementing Regulation (EU) No 540/2011, as regards the conditions of approval of the active substances clothianidin, thiamethoxam and imidacloprid, and prohibiting the use and sale of seeds treated with plant protection products containing those active substances, Off. J. Eur. Union L 139/12 (2013) 32013R0485 http://eur-lex.europa.eu/legal-content/EN/TXT/?qid=1484755697880&uri=CELEX:32013R0485, (2013) , Accessed date: 26 September 2018.

[8] European Food Safety Authority (EFSA), EFSA identifies risks to bees from neonicotinoids, Press release EFSA, Parma, 16 January 2013http://www.efsa.europa.eu/en/press/news/130116 , Accessed date: 26 September 2018.

[9] European Commission (EC), Commission Regulations (EU) 2018/781–785 of 29 May 2018, Off. J. Eur. Union L 132 (2018) L:2018:132:TOC https://eur-lex.europa.eu/legal-content/EN/TXT/?uri=OJ:L:2018:132:TOC, (2018) , Accessed date: 26 September 2018.

[10] E.P. Benton, J.F. Grant, R.J. Webster, R.J. Nichols, R.S. Cowles, A.F. Lagalante, C.I. Coots, Assessment of imidacloprid and its metabolites in foliage of Eastern hemlock multiple years following treatment for hemlock woolly adelgid, *Adelges tsugae* (Hemiptera: Adelgidae), in forested conditions, J. Econ. Entomol. 108 (2015) 2672–2682.

[11] M. Seifrtova, T. Halesova, K. Sulcova, K. Riddellova, T. Erban, Distributions of imidacloprid, imidacloprid-olefin and imidacloprid-urea in green plant tissues and roots of rapeseed (*Brassica napus*) from artificially contaminated potting soil, Pest Manag. Sci. 73 (2017) 1010–1016.

[12] S. Suchail, D. Guez, L.P. Belzunces, Discrepancy between acute and chronic toxicity induced by imidacloprid and its metabolites in *Apis mellifera*, Environ. Toxicol. Chem. 20 (2001) 2482–2486.

[13] F. Marletto, A. Patetta, A. Manino, Laboratory assessment of pesticide toxicity to bumblebees, Bull. Insectol. 56 (2003) 155–158.

[14] G. Rondeau, F. Sanchez-Bayo, H.A. Tennekes, A. Decourtye, R. Ramirez-Romero, N. Desneux, Delayed and time-cumulative toxicity of imidacloprid in bees, ants and termites, Sci. Rep. 4 (2014) 5566.

[15] G.P. Dively, M.S. Embrey, A. Kamel, D.J. Hawthorne, J.S. Pettis, Assessment of chronic sublethal effects of imidacloprid on honey bee colony health, PLoS One 10 (2015) e0118748.

[16] L. Bortolotti, R. Montanari, J. Marcelino, P. Medrzycki, S. Maini, C. Porrini, Effects of sub-lethal imidacloprid doses on the homing rate and foraging activity of honey bees, Bull. Insectol. 56 (2003) 63–67.

[17] A. Decourtye, C. Armengaud, M. Renou, J. Devillers, S. Cluzeau, M. Gauthier, M.-H. Pham-Deleguef, Imidacloprid impairs memory and brain metabolism in the honeybee, (*Apis mellifera L.*), Pestic. Biochem. Physiol. 78 (2004) 83–92.

[18] A. Decourtye, J. Devillers, S. Cluzeau, M. Charreton, M.-H. Pham-Delegue, Effects of imidacloprid and deltamethrin on associative learning in honeybees under semi-field and laboratory conditions, Ecotoxicol. Environ. Saf. 57 (2004) 410–419.

[19] S.M. Williamson, G.A. Wright, Exposure to multiple cholinergic pesticides impairs olfactory learning and memory in honeybees, J. Exp. Biol. 216 (2013) 1799–1807.

[20] A. Ciereszko, J. Wilde, G.J. Dietrich, M. Siuda, B. Bak, S. Judycka, H. Karol, Sperm parameters of honeybee drones exposed to imidacloprid, Apidologie 48 (2017) 211–222.

[21] M.I. Smodis Skerl, A. Gregorc, Heat shock proteins and cell death in situ localisation in hypopharyngeal glands of honeybee (*Apis mellifera carnica*) workers after imidacloprid or coumaphos treatment, Apidologie 41 (2010) 73–86.

[22] J.-N. Tasei, J. Lerin, G. Ripault, Sub-lethal effects of imidacloprid on bumblebees, *Bombus terrestris* (Hymenoptera: Apidae), during a laboratory feeding test, Pest Manag. Sci. 56 (2000) 784–788.

[23] P.R. Whitehorn, S. O'Connor, F.L. Wackers, D. Goulson, Neonicotinoid pesticide reduces bumble bee colony growth and queen production, Science 336 (2012) 351–352.

[24] C. Moffat, J.G. Pacheco, Sheila Sharp, A.J. Samson, K.A. Bollan, J. Huang, S.T. Buckland, C.N. Connolly, Chronic exposure to neonicotinoids increases neuronal vulnerability to mitochondrial dysfunction in the bumblebee (*Bombus terrestris*), FASEB J. 29 (2015) 2112–2119.

[25] C. Moffat, S.T. Buckland, A.J. Samson, R. McArthur, V. Chamosa Pino, K.A. Bollan, J.T.-J. Huang, C.N. Connolly, Neonicotinoids target distinct nicotinic acetylcholine receptors and neurons, leading to differential risks to bumblebees, Sci. Rep. 6 (2016) 24764.

[26] J.D. Crall, C.M. Switzer, R.L. Oppenheimer, A.N. Ford Versypt, B. Dey, A. Brown, M. Eyster, C. Guerin, N.E. Pierce, S.A. Combes, B.L. de Bivort, Neonicotinoid exposure disrupts bumblebee nest behavior, social networks, and thermoregulation, Science 362 (2018) 683–686.

[27] R.H. Parkinson, J.M. Little, J.R. Gray, A sublethal dose of a neonicotinoid insecticide disrupts visual processing and collision avoidance behaviour in *Locusta migratoria*, Sci. Rep. 7 (2017) 936.

[28] C. Manjon, B.J. Troczka, M. Zaworra, K. Beadle, E. Randall, G. Hertlein, K.S. Singh, C.T. Zimmer, R.A. Homem, B. Lueke, R. Reid, L. Kor, M. Kohler, J. Benting, M.S. Williamson, T.G.E. Davies, L.M. Field, C. Bass, R. Nauen, Unravelling the molecular determinants of bee sensitivity to neonicotinoid insecticides, Curr. Biol. 28 (2018) 1137–1143.

[29] A. Brandt, K. Grikscheit, R. Siede, R. Grosse, M.D. Meixner, R. Buchler, Immunosuppression in honeybee queens by the neonicotinoids thiacloprid and clothianidin, Sci. Rep. 7 (2017) 4673.

[30] F. Dondero, A. Negri, L. Boatti, F. Marsano, F. Mignone, A. Viarengo, Transcriptomic and proteomic effects of a neonicotinoid insecticide mixture in the marine mussel (*Mytilus galloprovincialis* Lam.), Sci. Total Environ. 408 (2010) 3775–3786.

[31] J. Meng, C. Zhang, X. Chen, Y. Cao, S. Shang, Differential protein expression in the susceptible and resistant *Myzus persicae* (Sulzer) to imidacloprid, Pestic, Biochem. Physiol. 115 (2014) 1–8.

[32] R.R. Rix, M.M. Ayyanath, G.C. Cutler, Sublethal concentrations of imidacloprid increase reproduction, alter expression of detoxification genes, and prime *Myzus persicae* for subsequent stress, J. Pest. Sci. 89 (2016) 581–589.

[33] Y. Pan, T. Peng, X. Gao, L. Zhang, C. Yang, J. Xi, X. Xin, R. Bi, Q. Shang, Transcriptomic comparison of thiamethoxam-resistance adaptation in resistant and susceptible strains of *Aphis gossypii* Glover, Comp. Biochem. Physiol. D Genomics Proteomics 13 (2015) 10–15.

[34] T. Masuda, M. Tomita, Y. Ishihama, Phase transfer surfactant-aided trypsin digestion for membrane proteome analysis, J. Proteome Res. 7 (2008) 731–740.

[35] M. Anastassiades, S.J. Lehotay, D. Stajnbaher, F.J. Schenck, Fast and easy multiresidue method employing acetonitrile extraction/partitioning and "dispersive solid-phase extraction" for the determination of pesticide residues in produce, J. AOAC Int. 86 (2003) 412–－431.

[36] A.S. Hebert, A.L. Richards, D.J. Bailey, A. Ulbrich, E.E. Coughlin, M.S. Westphall, J.J. Coon, The one hour yeast proteome, Mol. Cell. Proteomics 13 (2014) 339–347.

[37] T. Erban, K. Harant, J. Chalupnikova, F. Kocourek, J. Stara, Beyond the survival and death of the deltamethrin-threatened pollen beetle *Meligethes aeneus*: an in-depth proteomic study employing a transcriptome database, J. Proteome 150 (2017) 281–289.

[38] J. Cox, M.Y. Hein, C.A. Luber, I. Paron, N. Nagaraj, M. Mann, Accurate proteome-wide label-free quantification by delayed normalization and maximal peptide ratio extraction, termed MaxLFQ, Mol. Cell. Proteomics 13 (2014) 2513–2526.

[39] J. Cox, M. Mann, 1D and 2D annotation enrichment: a statistical method integrating quantitative proteomics with complementary high-throughput data, BMC Bioinformatics 13 (2012) S12.

[40] S. Tyanova, T. Temu, P. Sinitcyn, A. Carlson, M.Y. Hein, T. Geiger, M. Mann, J. Cox, The Perseus computational platform for comprehensive analysis of (prote)omics data, Nat. Methods 13 (2016) 731–740.

[41] A. Marchler-Bauer, Y. Bo, L. Han, J. He, C.J. Lanczycki, S. Lu, F. Chitsaz, M.K. Derbyshire, R.C. Geer, N.R. Gonzales, M. Gwadz, D.I. Hurwitz, F. Lu, G.H. Marchler, J.S. Song, N. Thanki, Z. Wang, R.A. Yamashita, D. Zhang, C. Zheng, L.Y. Geer, S.H. Bryant, CDD/SPARCLE: functional classification of proteins via subfamily domain architectures, Nucleic Acids Res. 45 (2017) D200–D203.

[42] M. Kanehisa, M. Furumichi, M. Tanabe, Y. Sato, K. Morishima, KEGG: new perspectives on genomes, pathways, diseases and drugs, Nucleic Acids Res. 45 (2017) D353–D361.

[43] D. Szklarczyk, A. Franceschini, S. Wyder, K. Forslund, D. Heller, J. Huerta-Cepas, M. Simonovic, A. Roth, A. Santos, K.P. Tsafou, M. Kuhn, P. Bork, L.J. Jensen, C. von Mering, STRING v10: protein-protein interaction networks, integrated over the tree

of life, Nucleic Acids Res. 43 (2015) D447–D452.
[44] D. Szklarczyk, J.H. Morris, H. Cook, M. Kuhn, S. Wyder, M. Simonovic, A. Santos, N.T. Doncheva, A. Roth, P. Bork, L.J. Jensen, C. von Mering, The STRING database in 2017: quality-controlled protein–protein association networks made broadly accessible, Nucleic Acids Res. 45 (2017) D362–D368.
[45] S.F. Altschul, W. Gish, W. Miller, E.W. Myers, D.J. Lipman, Basic local alignment search tool, J. Mol. Biol. 215 (1990) 403–410.
[46] X. Li, F. Lu, M.N. Trinh, P. Schmiege, J. Seemann, J. Wang, G. Blobel, 3.3 Å structure of Niemann–pick C1 protein reveals insights into the function of the C-terminal luminal domain in cholesterol transport, Proc. Natl. Acad. Sci. U. S. A. 114 (2017) 9116–9121.
[47] X. Li, J. Wang, E. Coutavas, H. Shi, Q. Hao, G. Blobel, Structure of human Niemann–pick C1 protein, Proc. Natl. Acad. Sci. U. S. A. 113 (2016) 8212–8217.
[48] J.P. Davies, Y.A. Ioannou, Topological analysis of Niemann–pick C1 protein reveals that the membrane orientation of the putative sterol-sensing domain is identical to those of 3-hydroxy-3-methylglutaryl-CoA reductase and sterol regulatory element binding protein cleavage-activating protein, J. Biol. Chem. 275 (2000) 24367–24374.
[49] M.A. Larkin, G. Blackshields, N.P. Brown, R. Chenna, P.A. McGettigan, H. McWilliam, F. Valentin, I.M. Wallace, A. Wilm, R. Lopez, J.D. Thompson, T.J. Gibson, D.G. Higgins, W. Clustal, Clustal X version 2.0, Bioinformatics 23 (2007) 2947–2948.
[50] A. Sali, Comparative protein modeling by satisfaction of spatial restraints, Mol. Med. Today 1 (1995) 270–277.
[51] R.A. Laskowski, M.W. MacArthur, D.S. Moss, J.M. Thornton, PROCHECK: a program to check the stereochemical quality of protein structures, J. Appl. Crystallogr. 26 (1993) 283–291.
[52] N. Guex, M.C. Peitsch, SWISS-MODEL and the Swiss-Pdb Viewer: an environment for comparative protein modeling, Electrophoresis 18 (1997) 2714–2723.
[53] O. Trott, A.J. Olson, AutoDock Vina: improving the speed and accuracy of docking with a new scoring function, efficient optimization, and multithreading, J. Comput. Chem. 31 (2010) 455–461.
[54] M.D. Hanwell, D.E. Curtis, D.C. Lonie, T. Vandermeersch, E. Zurek, G.R. Hutchison, Avogadro: an advanced semantic chemical editor, visualization, and analysis platform, J. Cheminform. 4 (2012) 17.
[55] R.A. Laskowski, M.B. Swindells, LigPlot+: multiple ligand–protein interaction diagrams for drug discovery, J. Chem. Inf. Model. 51 (2011) 2778–2786.
[56] R. Nauen, K. Tietjen, K. Wagner, A. Elbert, Efficacy of plant metabolites of imidacloprid against *Myzus persicae* and *Aphis gossypii* (Homoptera: Aphididae), Pestic. Sci. 52 (1998) 53–57.
[57] R. Nauen, U. Reckmann, S. Armborst, H.-P. Stupp, A. Elbert, Whitefly-active metabolites of imidacloprid: biological efficacy and translocation in cotton plants, Pestic. Sci. 55 (1999) 265–271.
[58] S. Suchail, D. Guez, L.P. Belzunces, Toxicity of imidacloprid and its metabolites in *Apis mellifera*, in: L.P. Belzunces, C. Pelissier, G.B. Lewis (Eds.), Hazards of Pesticides to Bees, INRA, Paris, 2001, pp. 121–126.
[59] S. Suchail, G. De Sousa, R. Rahmani, L.P. Belzunces, *In vivo* distribution and metabolisation of ^{14}C-imidacloprid in different compartments of *Apis mellifera* L, Pest Manag. Sci. 60 (2004) 1056–1062.
[60] S. Suchail, D. Guez, L.P. Belzunces, Degradation of imidacloprid in *Apis mellifera*, in: L.P. Belzunces, C. Pelissier, G.B. Lewis (Eds.), Hazards of Pesticides to Bees, INRA, Paris, 2001, pp. 298–299.
[61] S. Suchail, L. Debrauwer, L.P. Belzunces, Metabolism of imidacloprid in *Apis mellifera*, Pest Manag. Sci. 60 (2004) 291–296.
[62] E.B. Spencer, A. Bianchi, J. Widmer, L.A. Witters, Brain acetyl-CoA carboxylase: isozymic identification and studies of its regulation during development and altered nutrition, Biochem. Biophys. Res. Commun. 192 (1993) 820–825.
[63] J.L. Goldstein, M.S. Brown, Regulation of the mevalonate pathway, Nature 343 (1990) 425–430.
[64] E.S. Istvan, Structural mechanism for statin inhibition of 3-hydroxy-3-methylglutaryl coenzyme A reductase, Am. Heart J. 144 (2002) S27–S32.
[65] R.U. Svensson, S.J. Parker, L.J. Eichner, M.J. Kolar, M. Wallace, S.N. Brun, P.S. Lombardo, J.L. Van Nostrand, A. Hutchins, L. Vera, L. Gerken, J. Greenwood, S. Bhat, G. Harriman, W.F. Westlin, H.J. Harwood, A. Saghatelian, R. Kapeller, C.M. Metallo, R.J. Shaw, Inhibition of acetyl-CoA carboxylase suppresses fatty acid synthesis and tumor growth of non-small-cell lung cancer in preclinical models, Nat. Med. 22 (2016) 1108–1119.
[66] Y. Sakakura, H. Shimano, H. Sone, A. Takahashi, K. Inoue, H. Toyoshima, S. Suzuki, N. Yamada, Sterol regulatory element-binding proteins induce an entire pathway of cholesterol synthesis, Biochem. Biophys. Res. Commun. 286 (2001) 176–183.
[67] J.D. Horton, Sterol regulatory element-binding proteins: transcriptional activators of lipid synthesis, Biochem. Soc. Trans. 30 (2002) 1091–1095.
[68] M.S. Brown, J.L. Goldstein, The SREBP pathway: regulation of cholesterol metabolism by proteolysis of a membrane-bound transcription factor, Cell 89 (1997) 331–340.
[69] D. Yao, J. Luo, Q. He, H. Shi, J. Li, H. Wang, H. Xu, Z. Chen, Y. Yi, J.J. Loor, SCD1 alters long-chain fatty acid (LCFA) composition and its expression is directly regulated by SREBP-1 and PPARγ 1 in dairy goat mammary cells, J. Cell. Physiol. 232 (2017) 635–649.
[70] R. Niwa, Y.S. Niwa, Enzymes for ecdysteroid biosynthesis: their biological functions in insects and beyond, Biosci. Biotechnol. Biochem. 78 (2014) 1283–1292.
[71] R.B. Rawson, The SREBP pathway — insights from insigs and insects, Nat. Rev. Mol. Cell Biol. 4 (2003) 631–640.
[72] J.D. Horton, J.L. Goldstein, M.S. Brown, SREBPs: activators of the complete program of cholesterol and fatty acid synthesis in the liver, J. Clin. Invest. 109 (2002) 1125–1131.
[73] M. Tomizawa, J.E. Casida, Imidacloprid, thiacloprid, and their imine derivatives up-regulate the α4β2 nicotinic acetylcholine receptor in M10 cells, Toxicol. Appl. Pharmacol. 169 (2000) 114–120.
[74] M. Tomizawa, J.E. Casida, Desnitro-imidacloprid activates the extracellular signal-regulated kinase cascade via the nicotinic receptor and intracellular calcium mobilization in N1E-115 cells, Toxicol. Appl. Pharmacol. 184 (2002) 180–186.
[75] M. Cordero-Erausquin, L.M. Marubio, R. Klink, J.-P. Changeux, Nicotinic receptor function: new perspectives from knockout mice, Trends Pharmacol. Sci. 21 (2000) 211–217.
[76] A.K. Jones, D.B. Sattelle, Diversity of insect nicotinic acetylcholine receptor subunits, Adv. Exp. Med. Biol. 683 (2010) 25–43.
[77] M. Gauthier, State of the art on insect nicotinic acetylcholine receptor function in learning and memory, Adv. Exp. Med. Biol. 683 (2010) 97–115.
[78] H.M.V.S. Azevedo-Pereira, M.F.L. Lemos, A.M.V.M. Soares, Effects of imidacloprid exposure on *Chironomus riparius* Meigen larvae: linking acetylcholinesterase activity to behavior, Ecotoxicol. Environ. Saf. 74 (2011) 1210–1215.
[79] A.P. Beigneux, C. Kosinski, B. Gavino, J.D. Horton, W.C. Skarnes, S.G. Young, ATP-citrate lyase deficiency in the mouse, J. Biol. Chem. 279 (2004) 9557–9564.
[80] I. Buhaescu, H. Izzedine, Mevalonate pathway: a review of clinical and therapeutical implications, Clin. Biochem. 40 (2007) 575–584.
[81] M. Moutinho, M.J. Nunes, E. Rodrigues, The mevalonate pathway in neurons: it's not just about cholesterol, Exp. Cell Res. 360 (2017) 55–60.
[82] S. Zhao, R. Li, Y. Li, W. Chen, Y. Zhang, G. Chen, Roles of vitamin A status and retinoids in glucose and fatty acid metabolism, Biochem. Cell Biol. 90 (2012) 142–152.
[83] S. Yan, X.-F. Yang, H.-L. Liu, N. Fu, Y. Ouyang, K. Qing, Long-chain acyl-CoA synthetase in fatty acid metabolism involved in liver and other diseases: an update, World J. Gastroenterol. 21 (2015) 3492–3498.
[84] P. Zacek, D. Prchalova-Hornakova, R. Tykva, J. Kindl, H. Vogel, A. Svatos, I. Pichova, I. Valterova, De novo biosynthesis of sexual pheromone in the labial gland of bumblebee males, Chembiochem 14 (2013) 361–371.
[85] R. Benton, K.S. Vannice, L.B. Vosshall, An essential role for a CD36-related receptor in pheromone detection in *Drosophila*, Nature 450 (2007) 289–293.
[86] X. Jin, T.S. Ha, D.P. Smith, SNMP is a signaling component required for pheromone sensitivity in *Drosophila*, Proc. Natl. Acad. Sci. U. S. A. 105 (2008) 10996–11001.
[87] M. Helmkampf, E. Cash, J. Gadau, Evolution of the insect desaturase gene family with an emphasis on social Hymenoptera, Mol. Biol. Evol. 32 (2015) 456–471.
[88] P. Matouskova, A. Luxova, J. Matouskova, P. Jiros, A. Svatos, I. Valterova, I. Pichova, A Δ^9 desaturase from *Bombus lucorum* males: investigation of the biosynthetic pathway of marking pheromones, Chembiochem 9 (2008) 2534–2541.
[89] P. Barlow, R.M. Marchbanks, The effects of inhibiting choline dehydrogenase on choline metabolism in mice, Biochem. Pharmacol. 34 (1985) 3117–3122.
[90] Y. Ishida, Y. Kuwahara, M. Dadashipour, A. Ina, T. Yamaguchi, M. Morita, Y. Ichiki, Y. Asano, A sacrificial millipede altruistically protects its swarm using a drone blood enzyme, mandelonitrile oxidase, Sci. Rep. 6 (2016) 26998.
[91] L. Motteran, M.S. Pilone, G. Molla, S. Ghisla, L. Pollegioni, Cholesterol oxidase from *Brevibacterium sterolicum*: the relationship between covalent flavinylation and redox properties, J. Biol. Chem. 276 (2001) 18024–18030.
[92] A. Vrielink, L.F. Lloyd, D.M. Blow, Crystal structure of cholesterol oxidase from *Brevibacterium sterolicum* refined at 1.8 Å resolution, J. Mol. Biol. 219 (1991) 533–554.
[93] B.Q. Wei, T.S. Mikkelsen, M.K. McKinney, E.S. Lander, B.F. Cravatt, A second fatty acid amide hydrolase with variable distribution among placental mammals, J. Biol. Chem. 281 (2006) 36569–36578.
[94] J. McPartland, V. Di Marzo, L. De Petrocellis, A. Mercer, M. Glass, Cannabinoid receptors are absent in insects, J. Comp. Neurol. 436 (2001) 423–429.
[95] J.M. McPartland, J. Agraval, D. Gleeson, K. Heasman, M. Glass, Cannabinoid receptors in invertebrates, J. Evol. Biol. 19 (2006) 366–373.
[96] E. Demetz, A. Schroll, K. Auer, C. Heim, J.R. Patsch, P. Eller, M. Theurl, I. Theurl, M. Theurl, M. Seifert, D. Lener, U. Stanzl, D. Haschka, M. Asshoff, S. Dichtl, M. Nairz, E. Huber, M. Stadlinger, A.R. Moschen, X. Li, P. Pallweber, H. Scharnagl, T. Stojakovic, W. Marz, M.E. Kleber, K. Garlaschelli, P. Uboldi, A.L. Catapano, F. Stellaard, M. Rudling, K. Kuba, Y. Imai, M. Arita, J.D. Schuetz, P.P. Pramstaller, U.J.F. Tietge, M. Trauner, G.D. Norata, T. Claudel, A.A. Hicks, G. Weiss, I. Tancevski, The arachidonic acid metabolome serves as a conserved regulator of cholesterol metabolism, Cell Metab. 20 (2014) 787–798.
[97] A. Blanco-Grau, I. Bonaventura-Ibars, J. Coll-Canti, M.J. Melia, R. Martinez, M. Martinez-Gallo, A.L. Andreu, T. Pinos, E. Garcia-Arumi, Identification and biochemical characterization of the novel mutation m.8839G > C in the mitochondrial ATP6 gene associated with NARP syndrome, Genes Brain Behav. 12 (2013) 812–820.
[98] J. Horwitz, Alpha-crystallin, Exp. Eye Res. 76 (2003) 145–153.